

Self-Supervised Learning Based Handwriting Verification

Mihir Chauhan Mohammad Abuzar Shaikh Bina Ramamurthy
Mingchen Gao Siwei Lyu Sargur Srihari

Department of Computer Science and Engineering
The State University of New York, Buffalo, NY, USA

{mihirhem, mshaikh2, bina, mgao8, siweilyu, srihari}@buffalo.edu

Abstract

We present *SSL-HV: Self-Supervised Learning approaches applied to the task of Handwriting Verification*. This task involves determining whether a given pair of handwritten images originate from the same or different writer distribution. We have compared the performance of multiple generative, contrastive SSL approaches against handcrafted feature extractors and supervised learning on CEDAR AND dataset. We show that ResNet based Variational Auto-Encoder (VAE) outperforms other generative approaches achieving 76.3% accuracy, while ResNet-18 fine-tuned using Variance-Invariance-Covariance Regularization (VICReg) outperforms other contrastive approaches achieving 78% accuracy. Using a pre-trained VAE and VICReg for the downstream task of writer verification we observed a relative improvement in accuracy of 6.7% and 9% over ResNet-18 supervised baseline with 10% writer labels. Our code is available at <https://github.com/Mihir2/ssl-hv>.

1. Introduction

Handwriting Verification is the process of comparing questioned writing and known writing [59]. It is a critical task in various domains including forensics, banking, and legal proceedings. Traditional approaches to handwriting verification [65] includes using global handwriting features to determine between-writer and within-writer variations do not capture the full complexity and variability in handwriting. With the advent of artificial neural networks, deep networks like Convolutional Neural Networks (CNNs) and Vision Transformers (ViT) are used to generate hierarchical representation from images. Such networks have shown promising results on variety of vision tasks and there has been increasing amount of research being done to apply these deep learning techniques to the downstream tasks

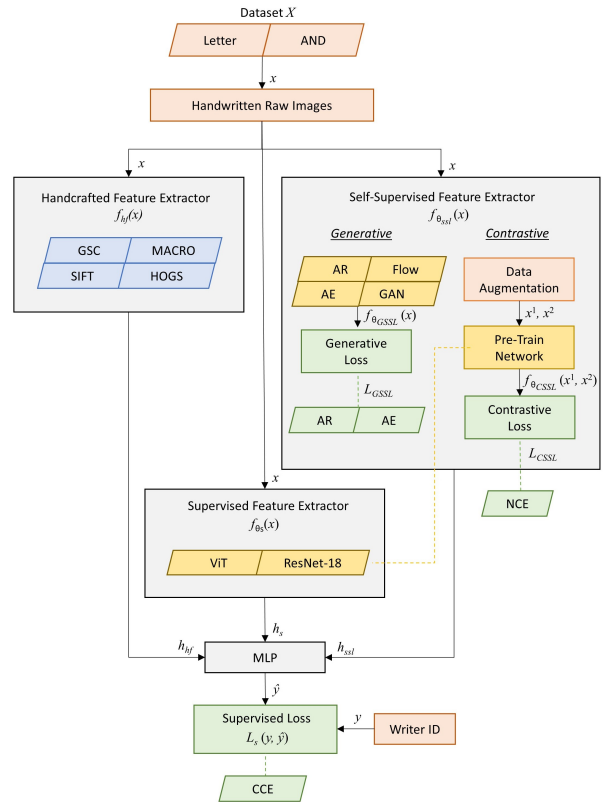


Figure 1. The overall framework for the SSL-HV for generating representation for the task of Handwriting Verification.

of Handwriting Identification, Writer-Retrieval and Recognition. Supervised approaches $f_{\theta_s}(x, y)$ [24] [64] [16] using deep networks heavily rely on supervised writer labels y during it's training process. Collecting a diverse dataset $X(x_q, x_k, y)$ with known x_k , questioned x_q handwritten samples and corresponding writer labels y is expensive and time-consuming. The dependency on labeled dataset limits the scalability of the supervised methods because of data collection and labeling efforts.

Self-Supervised Learning (SSL) [6] provides an alternative approach to learn meaningful representations from input X by leveraging the intrinsic patterns and structures from input X without the need of explicit supervised labels y . This helps to reduce the burden of data collection and allows the utilization of large amount of untapped unlabeled or partially labeled data that is available. Although, SSL has been employed in various domains within Computer Vision, but the application of SSL has been limited within handwriting domain.

Some examples of handwritten features generated using SSL are: SURDS [15] propose a two-staged SSL framework for writer independent Offline Signature Verification by using a dual triplet loss base fine tuning. The authors in [51] use a SSL for handwriting identification for medieval by finetuning a ResNet18 [43] architecture on a set of unlabeled manuscripts using Triplet Loss. POSM [55] uses SSL for pretraining models to extract representations from online handwriting in English and Chinese languages. The pretrained POSM models were capable of achieving good results on diverse set of handwriting tasks such as writer identification, handedness classification etc. The authors in [58] uses SSL approach with Vision Transformers (ViT) for writer retrieval task based on knowledge distillation. The authors also showcased the attention feature maps which elaborated different parts of the handwriting like loops, characters which enhanced the explainability for writer retrieval. More recently, CSSL-RHA [75] used Contrastive SSL for Handwriting Authentication. The authors use a hybrid CNN-Vit network for pre-training with momentum-based paradigm followed by projection head while minimizing a InfoNCE loss [73].

Motivated by the lack of SSL application to the domain of handwritten document representation, we apply SSL approaches $f_{\theta_{SSL}}(x)$ to generate representations h_{ssl} for the handwritten images (x_q, x_k) as shown in Figure 1. Our contributions: (1) We create a baseline for handwriting verification task using handcrafted features and supervised learning approach using ResNet-18 [43] and ViT [32]. (2) We pre-train using four Generative SSL (GSSL-HV) approaches for learning representations h_{ssl} for the downstream task of Handwriting Verification using Auto-Regressive Image Modeling [34], Flow based model [29] [30] [45], Masked AutoEncoder [41], ResNet based Variational AutoEncoders (VAE) [48] and Bi-Directional Generative Adversarial Network (Bi-GAN) [31]. (3) We pre-train eight Contrastive SSL (CSSL-HV) approaches using ResNet-18 [43] as encoder networks $f_{\theta}(x)$ to learn representations from handwritten images x . The contrastive approaches are MoCo [42], SimCLR [18], SimSiam [21], FastSiam [60], DINO [14], BarlowTwins [82] and VicReg [8]. (4) Lastly, we fine-tune a MLP $f_{\theta_{MLP}}(h_{SSL}, y)$ for the downstream task of handwriting verification on CEDAR AND dataset.


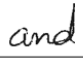
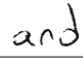
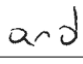
				
Sample ID [XXXXy_numZ]	0001a_num1	0001a_num2	0002a_num1	0002a_num2
Writer Number [XXXX]	Writer 0001	Writer 0001	Writer 0002	Writer 0002
Page Number [y]	Page 1	Page 1	Page 1	Page 1
Sample Number [Z]	Sample 1	Sample 2	Sample 1	Sample 2

Figure 2. Examples of “AND” image fragments extracted from CEDAR Letter dataset.

2. Dataset

CEDAR AND dataset is used for pre-training and fine-tuning on downstream task of verification. CEDAR AND dataset is derived from CEDAR Letter dataset wherein 1567 writers have written a letter manuscript three times. Each manuscript had up to five occurrences of the word “AND”. The manuscripts were passed to transcript-mapping tool of CEDAR-FOX [46] to extract image fragments of the word “AND”. In total, the tool was able to extract 15,518 image fragments of the word “AND”. Some examples of the snippets are shown in Figure 2. Each image was resized to 64x64 keeping uniform padding and aspect ratio.

Handcrafted features were derived for each “AND” image fragment. Gradient Structural Concavity (GSC) [35] features are used as micro features for forensic verification by CEDAR-FOX tool, a state-of-the-art handwriting analysis tool [66], developed at Center of Excellence for Document Analysis and Recognition, University at Buffalo. GSC features were extracted for the binarized “AND” images using a C-code. The GSC features are in 512 dimensions. CEDAR-FOX uses the GSC features to verify the log likelihood ratio (LLR) between the known and questioned handwritten sample. We use OpenCV HOGDescriptor for generating Histogram of Oriented Gradients (HOGs) [26] features for each AND image fragment. The HOGs features are 1764 dimensional vectors.

We use unseen writer data partitioning for supervised fine-tuning for downstream verification task. Hence, $W_{train} \cap W_{test} = \emptyset$, where W_{train} represents train writers and W_{test} represents test writers. For both pre-training and downstream fine-tuning, writer ids w_i up-to 1200 were used for training $i_{train} \in \{1, 2, \dots, 1200\}$ and rest were used as test. For fine-tuning, we generate equal number of same and different writer sample pairs. We have two setups for fine-tuning with 10% and 100% of train writers resulting in 13,232 and 129,602 pairs of known and questioned “AND” samples. The test is fixed for both setups with all the test writers $i_{test} > 1200$.

3. Learning Representation using Self-Supervised Learning based Pre-Training

Self-supervised learning (SSL) provides an opportunity to generate good representation for handwritten images without the need of supervised labels (writer ids). SSL has been used as a pre-text task for pre-training a network $f_{\theta_{SSL}}$ to generate representations h_{ssl} only using input data x without explicit writer labels y . SSL approaches either maximize the likelihood of unlabeled data $p(x)$ by reconstructing the input x from h or use a discriminative approach to learn representations by exploiting rich similarities between parts of input data. Hence, SSL approaches are mainly classified into Generative and Contrastive as summarized by Liu *et al.* in [53].

3.1. Generative SSL (GSSL)

Given input pairs (X, Y) where x_i is the i -th input example and y_i is i -th target/class label for x_i , generative approaches in statistics learns parameters θ from underlying probability distribution of $p(X)$ by maximizing likelihood of a generative objective function L . The parameters θ are optimized based on Maximum Likelihood Estimation (MLE), Bayesian Inference or adversarial training. SSL leverages the generative approaches to pre-train a network $f_{\theta}(x)$ which learns to generate hidden latent representation h by learning to fit on $P(X)$ by optimizing θ on L . The representations h learned during pre-training phase are used to train the downstream tasks with fewer labels Y .

Earliest work in the field of generative approach to learning representations and dimensionality reduction h are Deep Belief Networks [10], RBM [44] which uses a deep network whose parameters are updated using a reconstruction loss L_{recon} . Recently, significant advancements have been made in generative SSL approaches, leveraging techniques such as Auto-Regressive (AR) models, Flow-based models, Auto-Encoding models, and Generative Adversarial Networks (GANs).

AR Models can be considered directed probabilistic graphical models which models input data distribution $p(X) = p(x_1, \dots, x_n)$ as product of conditionals $\prod_{i=1}^n P(x_i | (x_1, \dots, x_{i-1}))$ where n is the input dimensionality. Many approaches have been proposed in the research to model the input image X distribution using product of pixel conditionals like NADE [70], RIDE [69], PixelRNN [71] and Gated PixelCNN [72]. We primarily use state-of-the-art AR model named Auto Regressive Image Modeling (AIM) which uses AutoRegressive loss function L_{AR} using Vision Transformer (ViT) [32] architecture. Given input data X the AR objective L_{AR} was to minimize the negative log likelihood of input distribution which is a density function modeled using product of n image patch conditionals. The prediction is a normalized pixel-level regression loss as

shown in Equation 1 below.

$$L_{AR} = \mathbb{E}_{x \sim X} [-\log \prod_{i=1}^n P(x_i | (x_1, \dots, x_{i-1}))] \quad (1)$$

$$\mathcal{L}_{recon} = \frac{1}{n} \sum_{i=1}^n \|\hat{x}_i - x_i\|^2$$

Flow based models explicitly learns the true data distribution $p(x)$ by a sequence of invertible transformation functions $f(x)$ to map input x to latent representation z . Since the transformation are invertible $x = f^{-1}(z)$ is true. Multiple flow based models like NICE [29], RealNVP [30], Glow [47] aim to provide a tractable and flexible solution to computing density function containing Jacobian determinant of the transformation. The loss is a negative log-likelihood over the input distribution dataset as shown in the Equation 2 below:

$$\log p_x(\mathbf{x}) = \log p_z(f(\mathbf{x})) + \log \left| \det \frac{df(\mathbf{x})}{d\mathbf{x}} \right| \quad (2)$$

Layers used in Flow based models shown in Figure 3 are variational dequantization to handle discrete pixel values in images to continuous values using uniform noise to each pixel, coupling layers helps to ensure invertibility of the forward and inverse transformation, squeeze and split operation helps in reducing the spatial resolution for efficiently training flow based models.

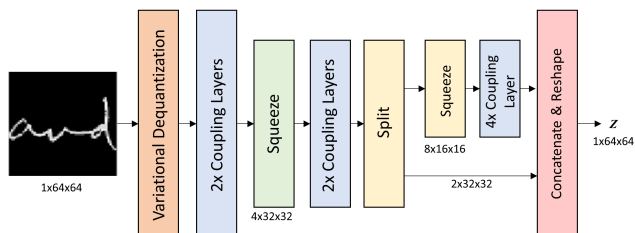


Figure 3. Flow based model architecture.

AutoEncoding Models AutoEncoder [7] transforms input x to latent representation z using an encoder feed forward neural network $z = f_{enc}(x)$. The latent representations z are then reconstructed using a decoder feed forward decoder network $x' = f_{dec}(z)$. The objective of the model is to regenerate x' which should be as close to x as possible from latent representations z . The loss is optimized using a reconstruction error $\mathcal{L}_{recon}(x, x')$ which could be mean squared error (MSE) as shown in Equation 3. The reconstruction loss could also be binary/categorical cross-entropy depending on the input data x and modality.

MAE Masked AutoEncoder [41] applies random mask patches M with high masking ratio on the input image x . Encoder $f_{enc}(x^m, p)$ is a Vision Transformer (ViT) [32]

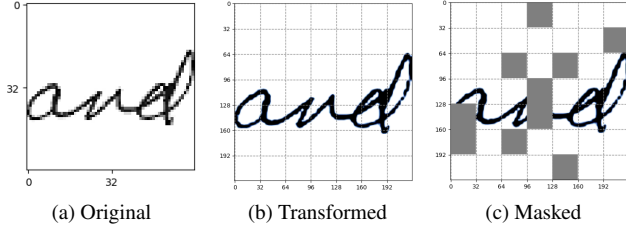


Figure 4. (a) Original AND image from writer 1471 first sample B with 64x64 size (b) Shows transformed image sample resized to 224x224 and normalized to ImageNet mean and std. deviation (b) Shows masked transformed image with 32x32 masked patches with masking ratio set to 0.2

which takes as input visible parts of the image x^m and positional embeddings p to generates latent representation z^m . A lightweight decoder $f_{dec}(z^m, p, M)$ reconstructs the entire image x including the missing patches using the encoded latent representations z^m of the masked image x^m , positional embeddings p and tokens from masked patches M . The loss is computed on the masked tokens patches only and is computed using Mean Squared Error (MSE) as shown in Equation 3.

$$\mathcal{L}_{recon} = \frac{1}{N^2} \sum_{i=1}^{N^2} \|x_i - f_{dec}(z_i^m, p_i, M_i)\|^2 \quad (3)$$

VAE Variational Auto Encoder belongs to class of Latent variable models (LVM). The goal of a latent generative model is to generate samples z from which we generate the most probable value of x according to the distribution $p(x|z)$. We first sample a value of z from some prior distribution $p(z)$ and then generate a sample from $p(x|z)$. Hence, our goal is to maximize the probability of x . The key to compute $p(x)$ is to attempt to sample values of z that are likely to have produced x using posterior probability $p(z|x)$. VAE minimizes the Reconstruction and Latent loss as shown in Equation 4. We can perform gradient-ascent on L_{vae} to update the generative and variational parameters.

$$L_{vae} = -E_{z \sim q_\phi(z|x)} [\log p_\theta(x|z)] + D_{KL}[q_\phi(z|x) || p_\theta(z)] \quad (4)$$

3.2. Contrastive SSL (CSSL)

Contrastive learning uses discriminative approach to learn representations h by maximizing the agreement between similar (positive) images and minimize the agreement between dissimilar (negative) images $P(Y|X = x)$. These discriminative model learns representation using Noise Contrastive Estimation (NCE) [39], InfoNCE [73] whose aim is to compare and learn the objective function

as shown in Eqn. 5 below:

$$\mathcal{L}_{nce} = -\log \frac{\exp[h_a^T \cdot h_+ / \tau]}{\exp[h_a^T \cdot h_+ / \tau] + \exp[h_a^T \cdot h_- / \tau]} \quad (5)$$

where, $h = f(x)$ are features and f is a function to embedding input x . x^+ is similar to input image used an an anchor x^a , x^- is dissimilar to x and f is a function to embed input image x to features h . Most contrastive SSL methods augmented views of the anchor image x^a as positive x^+ whereas all other images are used as negatives x^- .

Momentum Contrast (MoCo v1 [42], MoCo v2 [20], MoCo v3 [23]) maintains a dictionary of positive k_+ and negative k_i encoded-samples (keys) which is compared with the anchor (query) q . MoCo uses ResNet [43] as query f_q encoder and key f_k encoder parameterized by weights θ_f and θ_k with last Fully-Connected (FC) layer having 128-D fixed embeddings which are generated for each all Query and Keys. Further, InfoNCE [73] based loss function is used to measure the similarity between the query and key embeddings as shown in Equation 6 below:

$$\mathcal{L}_{moco} = -\log \frac{\exp(q \cdot k_+ / \tau)}{\sum_{i=0}^K \exp(q \cdot k_i / \tau)} \quad (6)$$

The parameters of the query f_q and key encoder f_k are update with a momentum parameters as: $\theta_k \leftarrow m\theta_k + (1 - m)\theta_q$ with m as momentum parameter. MoCo proposed v2 version by using using a MLP projection head and more data augmentation following the work of SimCLR [18].

Simple Contrastive Learning (SimCLR v1 [18], SimCLR v2 [19]) also learns representation by maximizing agreement between two differently augmented views x_i and x_j of the same example x . Specific augmentations types used were random cropping, color distrocutions and Gaurssian blur. Similar to MoCo, SimCLR also uses ReNet as the base encoder $h = f(x)$ where h is the average pooling layer from ResNet. Additionally, an MLP with 1 hidden layer and RELU activation function is used $z = g(h)$. The output of MLP are the latent embeddings z . The contrastive loss function for a pair of positive latent embeddings used is the normalized temperature-scaled cross entropy loss ($NT-Xent$) as shown in Equation 7 below:

$$\ell_{i,j} = -\log \frac{\exp(\text{sim}(z_i, z_j) / \tau)}{\sum_{k=1}^{2N} \mathbb{1}_{[k \neq i]} \exp(\text{sim}(z_i, z_k) / \tau)} \quad (7)$$

where, $\mathbb{1}_{[k \neq i]} \in 0, 1$, τ is temperature parameter and $\text{sim}(u, v)$ is the dot product between the l_2 normalized u and v .

Bootstrap Your Own Latent (BYOL) [38] removes the dependency on negative examples thereby being robust to batch size and memory constraints. BYOL uses an online and target network. Input to online network is first augmented view u of input. The online network consists of

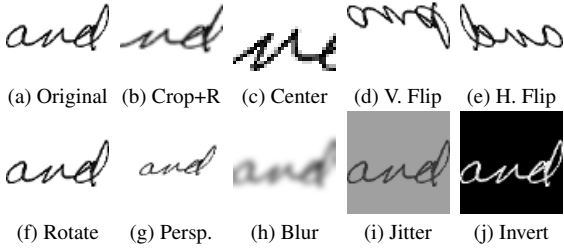


Figure 5. Data Augmentation Views from an example original image of word “AND” extracted from writer ID 1471-Sample-B1 from CEDAR Dataset.

an encoder $h_\theta = f_\theta(u_\theta)$, MLP projector $z_\theta = g_\theta(h_\theta)$ and predictor $q_\theta(z_\theta)$. The target network parameters ξ has the same architecture but uses moving average weights of the online parameters θ . After each training step, the weights are updated using $\xi \leftarrow \tau\xi + (1 - \tau)\theta$. The loss is mean squared error between the l_2 normalized predictions from the first augmented input-online network and the target network projections as shown in Equation 8:

$$\mathcal{L}_{\theta,\xi} \triangleq \|\overline{q_\theta(z_\theta)} - \overline{z'_\xi}\|_2^2 = 2 - 2 \cdot \frac{\langle q_\theta(z_\theta), z'_\xi \rangle}{\|q_\theta(z_\theta)\|_2 \cdot \|z'_\xi\|_2} \quad (8)$$

Simple Siamese (SimSiam) [21] simplifies BYOL [38] by maximizing contrastive between two augmented views x_1, x_2 of an example image x without negative pairs and without momentum encoder. The two views are processed by using ResNet [43] as an encoder f . Both the encoder share the same weights along with a MLP head p . x_1 is passed through the encoder f and MLP predictor p to get $p1 = p(f(x_1))$. Whereas, x_2 is only passed through f to get $z_2 = f(x_2)$. The loss is calculated as shown in the Equation 9 below:

$$\mathcal{L}_{SimSIAM} = \frac{1}{2}\mathcal{D}(p1, z_2) + \frac{1}{2}\mathcal{D}(p2, z1) \quad (9)$$

where,

$$\mathcal{D}(p1, z2) = -\frac{p1}{\|p1\|_2} \cdot \frac{z2}{\|z2\|_2} \quad (10)$$

Fast Siamese (FastSiam) [60] makes efficient use of SimSiam [21] approach by using multiple views of a single image, which allows for faster convergence and reduces amount of pre-training time.

Distillation with No Labels (DINO v1, v2) [14] [56] approach is similar to BYOL [38] and SimSIAM [21] where the idea is to use knowledge distillation. DINO trains a student network g_{θ_s} to imitate the output of the teacher network g_{θ_t} . A pair (x_1, x_2) of randomly augmented views of an image x are passed to student $s1 = g_{\theta_s}(x_1)$ and teacher $t1 = g_{\theta_t}(x_1)$. DINO uses Vision Transformers [32] or ResNet [43] for network g and 3-layer MLP followed by

l_2 normalization and a weight normalized FC layer with K dimensions. The resultant of passing the augmented images through network g followed by MLP is a output probability distributions over K dimensions as shown in the Equation 11 below:

$$P_s(x)^{(i)} = \frac{\exp(g_{\theta_s}(x)^{(i)}/\tau_s)}{\sum_{k=1}^K \exp(g_{\theta_s}(x)^{(k)}/\tau_s)} \quad (11)$$

In the above Equation 11 τ_s is a temperature parameter. DINO minimizes cross-entropy loss between probability distributions $P_s(x)$ and $P_t(x)$ generated by student and teacher networks as shown in the Equation 12 below:

$$\mathcal{L}_{DINO} = \min_{\theta_s} \sum_{x \in \{x_1^g, x_2^g\}} \sum_{x' \in V, x' \neq x} H(P_t(x), P_s(x')) \quad (12)$$

Where, $H(a, b) = -a \log b$. Furthermore, DINO uses Exponential Moving Averages on the student weights $\theta_t \leftarrow \lambda\theta_t + (1 - \lambda)\theta_s$ which is similar to momentum encoder ideas in MoCo [42].

Barlow Twins [82] makes use of cross-correlation matrix as shown in Equation 13 on a batch of mean-centered embeddings Z^A and Z^B generated by a network function f_θ from two augmented views $Y^A Y^B$ of the image X .

$$C_{ij} \triangleq \frac{\sum_b z_{b,i}^A z_{b,j}^B}{\sqrt{\sum_b (z_{b,i}^A)^2} \sqrt{\sum_b (z_{b,j}^B)^2}} \quad (13)$$

The encoder network uses ResNet [43] (without classification layer) followed by 3 layer MLP with 8192 output units. The goal is to make the cross-correlations between the outputs Z^A and Z^B closer to the identity matrix as shown in Loss Equation 14.

$$\mathcal{L}_{BT} \triangleq \underbrace{\sum_i (1 - C_{ii})^2}_{\text{invariance term}} + \lambda \underbrace{\sum_i \sum_{j \neq i} C_{ij}^2}_{\text{redundancy reduction term}} \quad (14)$$

Variance-Invariance-Covariance Regularization (VICReg, VICRegL) [8] [9]: tackles the model collapse problem - which happens when the model produces same representations irrespective of input. Similar to other approaches mentioned above, given an input image i , two augmented views x and x' are generated. Then using encoder network f_θ representations are generated. $y = f(x)$ and $y = f(x')$ which is then passed to expander to generate embeddings $z = h_\phi(x)$ and $z' = h_\phi(x')$. The loss between the embeddings z and z' is a weighted average of three terms in loss function as shown in Equation 15.

$$\ell(Z, Z') = \lambda \underbrace{s(Z, Z')}_{\text{Invariance}} + \mu \underbrace{[v(Z) + v(Z')]}_{\text{Variance}} + \nu \underbrace{[c(Z) + c(Z')]}_{\text{Covariance}} \quad (15)$$

Model	Accuracy	Precision	Recall	F1-Score
GSC [35]	0.71 / 0.78	0.69 / 0.81	0.72 / 0.77	0.69 / 0.79
ResNet-18 [43]	0.72 / 0.84	0.70 / 0.86	0.73 / 0.82	0.72 / 0.84
ViT [32]	0.65 / 0.79	0.68 / 0.80	0.64 / 0.78	0.66 / 0.79

Table 1. Performance Metrics on Test Writer (w_i where $i \geq 1200$) set for Supervised Baselines with 10% & 100% of Train Writers.

Variance is a regularization term acting as a hinge function on standard deviation of the embeddings Z . For covariance, VICReg uses covariance matrix term similar to BarlowTwin [82] and finally invariance criterion is a mean-squared euclidean distance between each pairs of vectors without normalization.

4. Experiments and Implementation Details

4.1. Supervised Baseline

Feature Extractors: Supervised baseline is performed using two handcrafted features (GSC, HOGs), CNN based ResNet-18 and Vision Transformer based ViT architecture on CEDAR AND dataset for 10% and 100% of train writers. ResNet-18 [43] CNN architecture having 11.2 M parameters is fine-tuned on the training pairs for each setup. With ResNet-18 we update the first convolutional layer to accept 3 channel input and set the last FC within ResNet-18 to be Identity and add a supervised classification head as elaborated in the next section. MaskedCausalVisionTransformer is used with configurations same as AIM which will be described in detail within the following sections on applying AIM to downstream verification task. ViT has 88.2M parameters.

Classification Head: The output of the feature extractors is fed into 2 fully-connected (FC) layers. FC1 and FC2 has 256 and 128 hidden neurons with ReLU activations. The final layer has 2 output neurons whose softmax activations represent similarity of samples with a one hot vector representation. We use categorical cross entropy loss given one-hot encoded logits compared to the target which is binary (0 or 1).

Training: Batch Size for training was 256, Learning rate $1e-3$, Adam Optimizer and Early stopping with F1 score stagnating with patience 5 and delta 0.001 for all baselines GSC, ViT and ResNet-18. The results from the supervised training with on 10% and 100% train writers are tabulated in Table 1.

Pre-Training Metric: In Table 2 shows multiple SSL methods and pre-training performance using the mean of intra-writer COS_{intra} and inter-writer cosine COS_{inter} similarity on a validation set.

$$COS(\mathbf{h}_k, \mathbf{h}_q) = \frac{\mathbf{h}_k \cdot \mathbf{h}_q}{\|\mathbf{h}_k\| \|\mathbf{h}_q\|} \quad (16)$$

In the Equation 16 above, \mathbf{h}_k represents the features of the handwritten sample from known writer and \mathbf{h}_q represents the features of the handwritten samples from questioned writer. COS_{intra} is when writer of Known and Questioned sample is same. COS_{inter} is when Known and Questioned sample is from different writers. This intra and inter cosine similarity separation evaluation metric was set to measure the separation between COS_{intra} and COS_{inter} during the pre-training phase in order to track SSL model capability to differentiate samples between writers. The separation provides a proxy metric to check for representation collapse and track the progress of pre-training. Intra-2d and Inter-2d shows the cosine similarity between and amongst test writers with writer ids greater than 1200. Intra-2d and Inter-2d are two dimensional representation obtained using TSNE dimensionality reduction. We then calculate the cosine similarity amongst test writers.

Downstream Verification Metric: We compare the downstream model performance using classification metrics such as accuracy to compare pre-trained SSL-HV model performance against handcrafted features and supervised models.

4.2. Generative Self-Supervised Learning for Handwriting Verification (GSSL-HV)

AIM [34] uses random masking to sequentially learn masked patches of the handwritten word AND using an autoregressive objective function. The input handwritten image of AND is divided into non-overlapping patches with 32 patch_size as shown in Figure 4c. AIM works well with simple data augmentations during training hence we used Resize by Torch [3] with size 224x224 because the ViT was trained on 224x224 image sizes. We normalize the image with mean (0.485, 0.456, 0.406) and standard deviation (0.229, 0.224, 0.225) which is same as used in the ImageNet dataset. For testing, same transformation are used as train. Output of the image transformations is shown in the Figure 4. We use CausalVisionTransformer as the backbone with masked causal attention based on AIM [34] at input image resolution 224x224. The sequence length for CausalVisionTransformer was 49 since the patch size was 32 with no [CLS] classification token. The embedding dimension of the encoder is 768, depth and number of attention heads 12. The encoder has 88.2M parameters. Projection head consists of a Linear FC layer followed by AIMPrediction-HeadBlock, LayerNorm and another Linear Layer. The projection head contains 41.4M parameters. The loss for AIM is Mean Square Error Loss which is same as MAE loss as shown in Equation 3. Optimizer is AdamW with learning rate $1.5e-4$. The batch_size was set to 1024 which takes 22.3GiB out of the total 24GiB of GPU memory.

Normalizing Flow model trained using a series of flow transformation to estimate the density of $p(x)$ using the la-

tent representation z with $p(z)$. The input handwritten AND image is inverted with and converted to gray-scale with a single channel and pixel value between [0,255]. Figure 3 shows the flow based architecture. We use a single variational de-quantization layer to quantize discrete pixel values as samples from continuous distribution which helps improve diversity and quality of generated samples. This is followed by 2 affine coupling layers [29] with a single channel checkerboard mask throughout the network. A Gated CNN using two-layer convolutional ResNet block with input gate is used similar to Flow++ [45]. We use multi-scale architecture as proposed by RealNVP [30] using Squeeze and Split layers. The batch_size for train and test is set to 128, Adam optimizer and learning rate set to 1e-3. The objective function is a negative log-likelihood function. The model is evaluated based using bits per dimension (bpd) for the train and validation set. Train and Val bpd was 0.8355 and 0.841 respectively. Total numbers of parameters are 1.7M and the 16GiB of GPU memory during training.

MAE is applied using random masking to reconstruct masked patches of the handwritten word AND. The masking ratio of removed patches was set to 20%. The input handwritten image of AND is divided into non-overlapping patches with 32 patch_size as shown in Figure 4c. Similar to AIM, MAE uses simple resizing to 224x224 and normalization with mean (0.485, 0.456, 0.406) and standard deviation (0.229, 0.224, 0.225) as used in the ImageNet dataset. For testing, we use the same transformation as train. Output of the image transformations is shown in the Figure 4. We use vit-base-patch32-224-in21k [77] as the backbone for MAE which is a Vision Transformer (ViT) trained on ImageNet-21k [27] at resolution 224x224. The embedding dimension of the encoder is 768. The encoder has 88M parameters. Decoder contains a linear layer which takes in the 768 dimensional embedding from the encoder and outputs 512 dimensional. The output of the linear layer is fed into a single Vision Transformer followed by normalization and linear layer. The final linear layer reconstructs the masked patches with outputs size as (patch_size, patch_size, num_channels). The decoder has 5.1M parameters. The loss for MAE is Mean Square Error Loss as shown in Equation 3. Optimizer is AdamW with learning rate 1e-3. The batch_size was set to 1024 which takes 16GiB out of the total 24GiB of GPU memory.

VAE takes as input an inverted image with size 64x64x3. The encoder f_{enc} and decoder f_{dec} used in VAE is the ResNet Encoder and Decoder by Pytorch Bolt [11]. The ResNet encoder f_{enc} output dimension 512 and has 11.2M trainable parameters while the f_{dec} has 8.6M parameters. f_{enc} is followed by two fully-connected layers FC_μ and FC_σ with 131k parameters as f_{enc} output dimensions are 512 and latent dimensions z are 256. The loss was computed using ELBO as described in the VAE section. The

learning rate was set to 1e-4 with Adam optimizer.

BiGan [31] is trained using an Encoder f_{enc} , Generator f_G and Discriminator f_D network. The f_{enc} network consists of 5 blocks, starting with 1024 hidden units and consequently layers have hidden units divided by 2. f_{enc} network which takes as input raw flattened image and outputs latent representation z with dimensionality as 100. Each block has a LeakyRelu activation and normalization except the first layer. The final activation layer has tanh activation to keep the value between -1 and 1. The f_G network takes as input z latent representation and also network structure which is opposite to the f_{enc} in order to re-generate back the output dimensions 64x64 with 3 channels. The discriminator takes as input image and latent representation and minimizes the binary cross-entropy loss between the fake and valid combination samples of latent representation and input image. We use pytorch lightning multi-optimizer function to update the gradients of generator and discriminator in an alternating fashion. The total number of parameters in generator and encoder are 26.6M while the discriminator has 6.9M parameters. Adam optimizer with learning rate set to 2e-4.

4.3. Contrastive Self-Supervised Learning for Handwriting Verification (CSSL-HV)

Data Augmentation regularizes the model and helps it to learn from patterns within different parts of the input image. There exists a wide variety of augmentation techniques which can be used to get different forms of invariances. Here, invariance is a property of the representation learning model to generate similar image embeddings/representations irrespective of the position, rotation, scale etc. of the image. Depending on the type of invariance requirement of the downstream task, we can apply these transforms (invariances) to the pre-training network. For example, since our domain is of handwriting verification pen and background color can be invariant. However, we should not randomize on aspect-ratio transformation or blurring in cases of handwriting because it will lead to underfitting and performance degradation. Some examples of invariances as mentioned and illustrated by SimCLR [18] are: Shape Invariances like Random Cropping, Random Horizontal/Vertical Flip, Rotation etc, Texture Invariances - Gaussian Blur and Color Invariance. The authors in [61] have shown the importance of data augmentation techniques in context of coarse-grained, fine-grained and few-shot downstream tasks. It is important to note that, for certain downstream fine-grained downstream tasks like that of differentiating between animal of same species like birds, we should not use color distortions like jitter, contrast etc. since the embeddings generated would underfit on the fine-grained downstream task as shown in [78]. In our case, we have used Pytorch Transforms [3] implementation for data augmentation with Lightly SSL framework [67].

Pre-Training, Projection Network and Loss Function

For pre-training network, we use a ResNet-18 [43] model with stochastic gradient descent with custom loss functions. We use 3x3 convolution kernel in the first few layers of ResNet-18 instead of originally proposed 7x7 kernel size for CEDAR AND dataset because it is well suited for small input images as in our case 64x64. ResNet-18 has 11.2M parameters. For CEDAR AND dataset we chose a larger kernel size 7x7 variant of ResNet-18 since the Crop size from augmentation is 224x224. The variant has also has 11.2M parameters. For the projection head/network and loss function, each CSSL approach described will have different number of neurons and layers in the projection network. MoCo [42] strategy was applied for pre-training a ResNet-18 [43] backbone network f_θ with 11.2M frozen weights θ . The backbone output is 512 dimensions which serves as the hidden representations for the down stream task. We then have projection head (328K weights) with momentum as described by MoCo [42]. The network minimizes the NTXent Loss as shown in Equation 6. We use transforms described by MoCo v2 [20] except turn off the RandomGaussian blur since the transform is too strong and underfits on the smaller resolution of the image. The batch size is set to 1024, memory bank size is 4096 and 200 number of epochs. With the given batch size and re-sized image to 45x45 20Gb out of 23Gb is consumed. The total pre-training time is 54 mins. For inference, 3GB memory GPU memory is consumed. SimCLR [18] was used for pre-training ResNet-18 [43] backbone. The output of backbone were 512 features. The backbone was followed by a projection head with (328k) weights and the loss was NTXent Loss. The transforms used were RandomResize (size 45x45) RandomHorizontalFlip, RandomVerticalFlip (0.5), RandomRotation(90 degrees), RandomGrayScale and GaussianBlur was not applied for the same reason as mentioned above. The batch size was 8000 to make sure that we are utilizing 23Gb of GPU memory during pretraining. During inference only 1.5Gb of memory was used. The total pretraining took 1h 7mins. BYOL [38] pretrains ResNet-18 to generate 512 features. The BYOL-Projection head contains 788k parameters and the loss criterion is NegativeCosineSimilarity. VicReg [8], BarlowTwins [82] and BYOL uses similar trasforms as SimCLR along with RandomSolarization applied. The batchsize was set to 1024 for 200 epochs. Similar to BYOL, FastSiam [60] and SimSiam [21] uses the same transforms except RandomSolarization and the batch size was set to 256 for both. DINO [14] global crop size was set to 45 rest of the transforms were the same as BYOL. All the experiments were conducted using Lightly SSL Python package [67] on AWS notebook instance with ml.g5.2xlarge which has 1 Nvidia A10G (24GB) GPU.

Model	Intra-Nd	Inter-Nd	Intra-2d	Inter-2d	Accuracy
Raw Pixels	0.96	0.95	0.07	-0.02	0.63
HOGS [26]	0.57	0.02	0.63	0.11	0.72
GSC [35]	0.92	0.67	0.86	0.56	0.71
AIM [34]	0.32	-0.05	0.78	0.75	0.73
Flow [29] [30] [45]	0.12	0.08	0.12	0.01	0.66
MAE [41]	0.18	0.02	0.82	0.77	0.71
VAE [49]	0.24	0.06	0.38	0.30	0.75
BiGAN [31]	0.35	0.30	0.27	0.25	0.68
MoCo [42]	0.89	0.78	0.92	0.73	0.73
SimClr [18]	0.89	0.87	0.87	0.85	0.72
BYOL [38]	0.88	0.84	0.91	0.97	0.73
SimSiam [21]	0.87	0.81	0.94	0.84	0.75
FastSiam [60]	0.83	0.75	0.83	0.75	0.71
DINO [14]	0.88	0.85	0.78	0.74	0.68
BarlowTwins [82]	0.87	0.79	0.66	0.38	0.76
VicReg [8]	0.69	0.48	0.65	0.60	0.78

Table 2. Performance comparison of GSSL-HV and CSSL-HV approaches against handcrafted feature baselines on CEDAR AND Dataset with 10% train writers.

5. Results

Table 2 shows the performance of the SSL and baseline approaches. We observe that higher the separation between writers (Intra distance - Inter distance) leads to higher test accuracy on a small training dataset. In the experiments performed we observe VAE to be best performing with a good separation of 0.18 between the intra-inter distance between and amongst the writers during the pre-training phase which lead to 6.7% relative increase in the accuracy when compared to the best performing supervised ResNet-18 baseline with accuracy 72% accuracy on 10% train writers. Auto-Regressive AIM model and MAE outperformed it’s supervised counterpart ViT on 10% train writers but had a lower precision compared to VAE which is contributed to the difference in the feature extraction process. Within VAE we used ResNet-18 architecture whereas AIM and MAE uses a ViT architecture whose baseline metrics under performed when compared to ResNet-18 as shown in Table 1. Flow based models performed similar to the baselines but underperformed when compared to VAE and AIM. This is contributed to the fact that flow based models do not support sparsity in feature representation and the type of invertible transformations are not suitable for granular variations within handwritten styles. GANs also performed similar to baselines, this may be primarily due to the fact that GANs are primarily used for data generation and do not naturally include an encoder to map data back to the latent space. We observed that GSC and HOGS features have maximum separation between COS_{intra} and COS_{inter} whereas using raw pixels the separability is very low. From the table 2 maximum separation of 0.28 is obtained using VicReg on the CEDAR AND Dataset leading to 9% relative improvement in accuracy over best performing supervised ResNet-18 baseline.

6. Conclusion

In conclusion, self-supervised learning provides a pathway to generating robust handwritten features which helps improve downstream task of handwriting verification with limited amount of training labels. In this paper, we evaluated AutoRegressive, Flow Based, AutoEncoding and GANs as part of the GSSL-HV framework. We also compared performance of eight CSSL-HV approaches. VAE outperformed other generative self-supervised feature extraction approaches, achieving a relative gain of 6.73% in accuracy whereas VICReg was outperformed all the generative and contrastive approaches with a relative accuracy gain of 9% over the baselines. Future research can aim to enhance the feature extraction capabilities using multiple unlabeled handwritten datasets such as IAM handwriting dataset and comparing similar and different handwritten content using state-of-the-art self-supervised approaches.

References

- [1] Alexander A. Alemi, Ben Poole, Ian Fischer, Joshua V. Dillon, Rif A. Saurous, and Kevin Murphy. Fixing a broken elbo, 2018. [14](#)
- [2] Alec Radford Jeffrey Wu Rewon Child David Luan Dario Amodei and Ilya Sutskever. Language models are unsupervised multitask learners. technical report., 2019. [13](#)
- [3] Jason Ansel, Edward Yang, Horace He, Natalia Gimelshein, Animesh Jain, Michael Voznesensky, Bin Bao, Peter Bell, David Berard, Evgeni Burovski, Geeta Chauhan, Anjali Chourdia, Will Constable, Alban Desmaison, Zachary DeVito, Elias Ellison, Will Feng, Jiong Gong, Michael Gschwind, Brian Hirsh, Sherlock Huang, Kshiteej Kalam-barkar, Laurent Kirsch, Michael Lazos, Mario Lezcano, Yanbo Liang, Jason Liang, Yinghai Lu, CK Luk, Bert Maher, Yunjie Pan, Christian Puhersch, Matthias Reso, Mark Saroufim, Marcos Yukio Siraichi, Helen Suk, Michael Suo, Phil Tillet, Eikan Wang, Xiaodong Wang, William Wen, Shunting Zhang, Xu Zhao, Keren Zhou, Richard Zou, Ajit Mathews, Gregory Chanan, Peng Wu, and Soumith Chintala. PyTorch 2: Faster Machine Learning Through Dynamic Python Bytecode Transformation and Graph Compilation. In *29th ACM International Conference on Architectural Support for Programming Languages and Operating Systems, Volume 2 (ASPLOS '24)*. ACM, Apr. 2024. [6](#), [7](#)
- [4] Mahmoud Assran, Randall Balestriero, Quentin Duval, Florian Bordes, Ishan Misra, Piotr Bojanowski, Pascal Vincent, Michael Rabbat, and Nicolas Ballas. The hidden uniform cluster prior in self-supervised learning, 2022. [14](#)
- [5] Mahmoud Assran, Mathilde Caron, Ishan Misra, Piotr Bojanowski, Florian Bordes, Pascal Vincent, Armand Joulin, Michael Rabbat, and Nicolas Ballas. Masked siamese networks for label-efficient learning, 2022. [14](#)
- [6] Randall Balestriero, Mark Ibrahim, Vlad Sobal, Ari Morcos, Shashank Shekhar, Tom Goldstein, Florian Bordes, Adrien Bardes, Gregoire Mialon, Yuandong Tian, Avi Schwarzschild, Andrew Gordon Wilson, Jonas Geiping, Quentin Garrido, Pierre Fernandez, Amir Bar, Hamed Pirsiavash, Yann LeCun, and Micah Goldblum. A cookbook of self-supervised learning, 2023. [2](#)
- [7] Dana H. Ballard. Modular learning in neural networks. In *Proceedings of the Sixth National Conference on Artificial Intelligence - Volume 1, AAAI'87*, page 279–284. AAAI Press, 1987. [3](#)
- [8] Adrien Bardes, Jean Ponce, and Yann LeCun. Vicreg: Variance-invariance-covariance regularization for self-supervised learning, 2022. [2](#), [5](#), [8](#)
- [9] Adrien Bardes, Jean Ponce, and Yann LeCun. Vicregl: Self-supervised learning of local visual features, 2022. [5](#)
- [10] Yoshua Bengio, Pascal Lamblin, Dan Popovici, and Hugo Larochelle. Greedy layer-wise training of deep networks. In B. Schölkopf, J. Platt, and T. Hoffman, editors, *Advances in Neural Information Processing Systems*, volume 19. MIT Press, 2006. [3](#)
- [11] Jirka Borovec, William Falcon, Akihiro Nitta, Ananya Harsh Jha, otaj, Annika Brundyn, Donal Byrne, Nathan Raw, Shion Matsumoto, Teddy Koker, Brian Ko, Aditya Oke, Sidhant Sundrani, Baruch, Christoph Clement, Clément POIRET, Rohit Gupta, Haswanth Aekula, Adrian Wälchli, Atharva Phatak, Ido Kessler, Jason Wang, JongMok Lee, Shivam Mehta, Zhengyu Yang, Garry O'Donnell, and zlapp. Lightning-ai/lightning-bolts: Minor patch release, dec 2022. [7](#)
- [12] Samuel R. Bowman, Luke Vilnis, Oriol Vinyals, Andrew M. Dai, Rafal Jozefowicz, and Samy Bengio. Generating sentences from a continuous space, 2016. [14](#)
- [13] Mathilde Caron, Ishan Misra, Julien Mairal, Priya Goyal, Piotr Bojanowski, and Armand Joulin. Unsupervised learning of visual features by contrasting cluster assignments, 2021. [14](#)
- [14] Mathilde Caron, Hugo Touvron, Ishan Misra, Hervé Jégou, Julien Mairal, Piotr Bojanowski, and Armand Joulin. Emerging properties in self-supervised vision transformers, 2021. [2](#), [5](#), [8](#)
- [15] Soumitri Chattopadhyay, Siladitya Manna, Saumik Bhattacharya, and Umapada Pal. Surds: Self-supervised attention-guided reconstruction and dual triplet loss for writer independent offline signature verification, 2022. [2](#)
- [16] Mihir Chauhan, Mohammad Abuzar Shaikh, and Sargur N. Srihari. Explanation based handwriting verification, 2019. [1](#)
- [17] Mark Chen, Alec Radford, Jeff Wu, Heewoo Jun, Prafulla Dhariwal, David Luan, and Ilya Sutskever. Generative pre-training from pixels. In *International Conference on Machine Learning*, 2020. [13](#)
- [18] Ting Chen, Simon Kornblith, Mohammad Norouzi, and Geoffrey Hinton. A simple framework for contrastive learning of visual representations, 2020. [2](#), [4](#), [7](#), [8](#), [14](#)
- [19] Ting Chen, Simon Kornblith, Kevin Swersky, Mohammad Norouzi, and Geoffrey Hinton. Big self-supervised models are strong semi-supervised learners, 2020. [4](#)
- [20] Xinlei Chen, Haoqi Fan, Ross Girshick, and Kaiming He. Improved baselines with momentum contrastive learning, 2020. [4](#), [8](#)
- [21] Xinlei Chen and Kaiming He. Exploring simple siamese representation learning, 2020. [2](#), [5](#), [8](#)

- [22] Xi Chen, Nikhil Mishra, Mostafa Rohaninejad, and Pieter Abbeel. Pixelsnail: An improved autoregressive generative model, 2017. [13](#)
- [23] Xinlei Chen, Saining Xie, and Kaiming He. An empirical study of training self-supervised vision transformers, 2021. [4](#)
- [24] Jun Chu, Mohammad Abuzar Shaikh, Mihir Chauhan, Lu Meng, and Sargur Srihari. Writer verification using cnn feature extraction. In *2018 16th International Conference on Frontiers in Handwriting Recognition (ICFHR)*, pages 181–186, 2018. [1](#)
- [25] Elijah Cole, Xuan Yang, Kimberly Wilber, Oisín Mac Aodha, and Serge Belongie. When does contrastive visual representation learning work?, 2022. [12](#)
- [26] N. Dalal and B. Triggs. Histograms of oriented gradients for human detection. In *2005 IEEE Computer Society Conference on Computer Vision and Pattern Recognition (CVPR'05)*, volume 1, pages 886–893 vol. 1, 2005. [2, 8](#)
- [27] Jia Deng, Wei Dong, Richard Socher, Li-Jia Li, Kai Li, and Li Fei-Fei. Imagenet: A large-scale hierarchical image database. In *2009 IEEE conference on computer vision and pattern recognition*, pages 248–255. Ieee, 2009. [7](#)
- [28] Jacob Devlin, Ming-Wei Chang, Kenton Lee, and Kristina Toutanova. Bert: Pre-training of deep bidirectional transformers for language understanding, 2019. [13](#)
- [29] Laurent Dinh, David Krueger, and Yoshua Bengio. Nice: Non-linear independent components estimation, 2015. [2, 3, 7, 8, 13](#)
- [30] Laurent Dinh, Jascha Sohl-Dickstein, and Samy Bengio. Density estimation using real nvp, 2017. [2, 3, 7, 8, 13](#)
- [31] Jeff Donahue, Philipp Krähenbühl, and Trevor Darrell. Adversarial feature learning, 2017. [2, 7, 8](#)
- [32] Alexey Dosovitskiy, Lucas Beyer, Alexander Kolesnikov, Dirk Weissenborn, Xiaohua Zhai, Thomas Unterthiner, Mostafa Dehghani, Matthias Minderer, Georg Heigold, Sylvain Gelly, Jakob Uszkoreit, and Neil Houlsby. An image is worth 16x16 words: Transformers for image recognition at scale, 2021. [2, 3, 5, 6](#)
- [33] Debidatta Dwibedi, Yusuf Aytar, Jonathan Tompson, Pierre Sermanet, and Andrew Zisserman. With a little help from my friends: Nearest-neighbor contrastive learning of visual representations, 2021. [14](#)
- [34] Alaaeldin El-Nouby, Michal Klein, Shuangfei Zhai, Miguel Angel Bautista, Alexander Toshev, Vaishaal Shankar, Joshua M Susskind, and Armand Joulin. Scalable pre-training of large autoregressive image models, 2024. [2, 6, 8](#)
- [35] John T. Favata and Geetha Srikanthan. A multiple feature/resolution approach to handprinted digit and character recognition. *International Journal of Imaging Systems and Technology*, 7(4):304–311, 1996. [2, 6, 8](#)
- [36] Ian J. Goodfellow, Jean Pouget-Abadie, Mehdi Mirza, Bing Xu, David Warde-Farley, Sherjil Ozair, Aaron Courville, and Yoshua Bengio. Generative adversarial networks, 2014. [14](#)
- [37] Alex Graves and Jürgen Schmidhuber. Offline handwriting recognition with multidimensional recurrent neural networks. In D. Koller, D. Schuurmans, Y. Bengio, and L. Bottou, editors, *Advances in Neural Information Processing Systems*, volume 21. Curran Associates, Inc., 2008. [12](#)
- [38] Jean-Bastien Grill, Florian Strub, Florent Altché, Corentin Tallec, Pierre H. Richemond, Elena Buchatskaya, Carl Doersch, Bernardo Avila Pires, Zhaohan Daniel Guo, Mohammad Gheshlaghi Azar, Bilal Piot, Koray Kavukcuoglu, Rémi Munos, and Michal Valko. Bootstrap your own latent: A new approach to self-supervised learning, 2020. [4, 5, 8](#)
- [39] Michael U. Gutmann and Aapo Hyvärinen. Noise-contrastive estimation of unnormalized statistical models, with applications to natural image statistics. *J. Mach. Learn. Res.*, 13(null):307–361, feb 2012. [4](#)
- [40] David Ha and Douglas Eck. A neural representation of sketch drawings, 2017. [14](#)
- [41] Kaiming He, Xinlei Chen, Saining Xie, Yanghao Li, Piotr Dollár, and Ross Girshick. Masked autoencoders are scalable vision learners, 2021. [2, 3, 8](#)
- [42] Kaiming He, Haoqi Fan, Yuxin Wu, Saining Xie, and Ross Girshick. Momentum contrast for unsupervised visual representation learning, 2020. [2, 4, 5, 8](#)
- [43] Kaiming He, Xiangyu Zhang, Shaoqing Ren, and Jian Sun. Deep residual learning for image recognition. *CoRR*, abs/1512.03385, 2015. [2, 4, 5, 6, 8](#)
- [44] Y. W. Hinton G. E. Osindero S. & Teh. A fast learning algorithm for deep belief nets., 2006. [3](#)
- [45] Jonathan Ho, Xi Chen, Aravind Srinivas, Yan Duan, and Pieter Abbeel. Flow++: Improving flow-based generative models with variational dequantization and architecture design, 2019. [2, 7, 8](#)
- [46] Chen Huang and Sargur N. Srihari. Mapping Transcripts to Handwritten Text. In Guy Lorette, editor, *Tenth International Workshop on Frontiers in Handwriting Recognition*, La Baule (France), Oct. 2006. Université de Rennes 1, Suvisoft. <http://www.suvisoft.com>. [2](#)
- [47] Diederik P. Kingma and Prafulla Dhariwal. Glow: Generative flow with invertible 1x1 convolutions, 2018. [3, 13](#)
- [48] Diederik P. Kingma and Max Welling. Auto-encoding variational bayes. *CoRR*, abs/1312.6114, 2014. [2](#)
- [49] Diederik P Kingma and Max Welling. Auto-encoding variational bayes, 2022. [8](#)
- [50] Alex Krizhevsky, Ilya Sutskever, and Geoffrey E. Hinton. Imagenet classification with deep convolutional neural networks. In *Proceedings of the 25th International Conference on Neural Information Processing Systems - Volume 1*, NIPS'12, pages 1097–1105, USA, 2012. Curran Associates Inc. [12, 14](#)
- [51] Lorenzo Lastilla, Serena Ammirati, Donatella Firmani, Nikos Komodakis, Paolo Meriardo, and Simone Scardapane. Self-supervised learning for medieval handwriting identification: A case study from the Vatican Apostolic Library. *Information Processing & Management*, 59(3):102875, 2022. [2](#)
- [52] Phillip Lippe. UvA Deep Learning Tutorials. <https://uvadlc-notebooks.readthedocs.io/en/latest/>, 2024. [13](#)
- [53] Xiao Liu, Fanjin Zhang, Zhenyu Hou, Li Mian, Zhaoyu Wang, Jing Zhang, and Jie Tang. Self-supervised learning:

- Generative or contrastive. *IEEE Transactions on Knowledge and Data Engineering*, page 1–1, 2021. 3
- [54] Alejandro López-Cifuentes, Marcos Escudero-Viñolo, Jesús Bescós, and Álvaro García-Martín. Semantic-aware scene recognition. *Pattern Recognition*, 102:107256, June 2020. 12
- [55] Pouya Mehralian, Bagher BabaAli, and Ashena Gorgan Mohammadi. Self-supervised representation learning for online handwriting text classification, 2023. 2
- [56] Maxime Oquab, Timothée Darcet, Théo Moutakanni, Huy Vo, Marc Szafraniec, Vasil Khalidov, Pierre Fernandez, Daniel Haziza, Francisco Massa, Alaaeldin El-Nouby, Mahmoud Assran, Nicolas Ballas, Wojciech Galuba, Russell Howes, Po-Yao Huang, Shang-Wen Li, Ishan Misra, Michael Rabbat, Vasu Sharma, Gabriel Synnaeve, Hu Xu, Hervé Jegou, Julien Mairal, Patrick Labatut, Armand Joulin, and Piotr Bojanowski. Dinov2: Learning robust visual features without supervision, 2024. 5
- [57] Bo Pang, Yifan Zhang, Yaoyi Li, Jia Cai, and Cewu Lu. Unsupervised visual representation learning by synchronous momentum grouping, 2022. 14
- [58] Marco Peer, Florian Kleber, and Robert Sablatnig. Self-supervised vision transformers with data augmentation strategies using morphological operations for writer retrieval. In *Frontiers in Handwriting Recognition: 18th International Conference, ICFHR 2022, Hyderabad, India, December 4–7, 2022, Proceedings*, page 122–136, Berlin, Heidelberg, 2022. Springer-Verlag. 2
- [59] R. Plamondon and S.N. Srihari. Online and off-line handwriting recognition: a comprehensive survey. *IEEE Transactions on Pattern Analysis and Machine Intelligence*, 22(1):63–84, 2000. 1
- [60] Daniel Pototzky, Azhar Sultan, and Lars Schmidt-Thieme. Fastiam: Resource-efficient self-supervised learning on a single gpu. In Björn Andres, Florian Bernard, Daniel Cremers, Simone Frintrop, Bastian Goldlücke, and Ivo Ihrke, editors, *Pattern Recognition*, pages 53–67, Cham, 2022. Springer International Publishing. 2, 5, 8
- [61] Senthil Purushwalkam and Abhinav Gupta. Demystifying contrastive self-supervised learning: Invariances, augmentations and dataset biases, 2020. 7
- [62] Ali Razavi, Aaron van den Oord, and Oriol Vinyals. Generating diverse high-fidelity images with vq-vae-2, 2019. 14
- [63] Tim Salimans, Andrej Karpathy, Xi Chen, and Diederik P. Kingma. Pixelcnn++: Improving the pixelcnn with discretized logistic mixture likelihood and other modifications, 2017. 13
- [64] Mohammad Abuzar Shaikh, Mihir Chauhan, Jun Chu, and Sargur Srihari. Hybrid feature learning for handwriting verification. In *2018 16th International Conference on Frontiers in Handwriting Recognition (ICFHR)*, pages 187–192, 2018. 1
- [65] S.N. Srihari, Sung-Hyuk Cha, H. Arora, and Sangjik Lee. Individuality of handwriting: a validation study. In *Proceedings of Sixth International Conference on Document Analysis and Recognition*, pages 106–109, 2001. 1
- [66] Sargur N. Srihari, Barish Srinivasan, and Kartik Desai. Questioned document examination using cedar-fox. *Journal of Forensic Document Examination*, 28:15–26, Dec. 2018. 2
- [67] Igor Susmelj, Matthias Heller, Philipp Wirth, Jeremy Prescott, and Malte Ebner et al. Lightly. *GitHub. Note: https://github.com/lightly-ai/lightly*, 2020. 7, 8
- [68] Casper Kaae Sønderby, Tapani Raiko, Lars Maaløe, Søren Kaae Sønderby, and Ole Winther. Ladder variational autoencoders, 2016. 14
- [69] Lucas Theis and Matthias Bethge. Generative image modeling using spatial lstms. In *Proceedings of the 28th International Conference on Neural Information Processing Systems - Volume 2, NIPS’15*, page 1927–1935, Cambridge, MA, USA, 2015. MIT Press. 3
- [70] Benigno Uria, Marc-Alexandre Côté, Karol Gregor, Iain Murray, and Hugo Larochelle. Neural autoregressive distribution estimation, 2016. 3
- [71] Aaron van den Oord, Nal Kalchbrenner, and Koray Kavukcuoglu. Pixel recurrent neural networks, 2016. 3, 12, 13
- [72] Aaron van den Oord, Nal Kalchbrenner, Oriol Vinyals, Lasse Espeholt, Alex Graves, and Koray Kavukcuoglu. Conditional image generation with pixelcnn decoders, 2016. 3, 12, 13
- [73] Aaron van den Oord, Yazhe Li, and Oriol Vinyals. Representation learning with contrastive predictive coding, 2019. 2, 4, 14
- [74] Aaron van den Oord, Oriol Vinyals, and Koray Kavukcuoglu. Neural discrete representation learning, 2018. 14
- [75] Jingyao Wang, Luntian Mou, Changwen Zheng, and Wen Gao. Cssl-rha: Contrastive self-supervised learning for robust handwriting authentication, 2023. 2
- [76] Liwei Wang, Alexander G. Schwing, and Svetlana Lazebnik. Diverse and accurate image description using a variational auto-encoder with an additive gaussian encoding space, 2017. 14
- [77] Bichen Wu, Chenfeng Xu, Xiaoliang Dai, Alvin Wan, Peizhao Zhang, Zhicheng Yan, Masayoshi Tomizuka, Joseph Gonzalez, Kurt Keutzer, and Peter Vajda. Visual transformers: Token-based image representation and processing for computer vision, 2020. 7
- [78] Tete Xiao, Xiaolong Wang, Alexei A. Efros, and Trevor Darrell. What should not be contrastive in contrastive learning, 2021. 7
- [79] Zichao Yang, Zhiting Hu, Ruslan Salakhutdinov, and Taylor Berg-Kirkpatrick. Improved variational autoencoders for text modeling using dilated convolutions, 2017. 14
- [80] Chun-Hsiao Yeh, Cheng-Yao Hong, Yen-Chi Hsu, Tyng-Luh Liu, Yubei Chen, and Yann LeCun. Decoupled contrastive learning, 2022. 14
- [81] Thomas Yerxa, Yilun Kuang, Eero Simoncelli, and Sueyeon Chung. Learning efficient coding of natural images with maximum manifold capacity representations, 2023. 14
- [82] Jure Zbontar, Li Jing, Ishan Misra, Yann LeCun, and Stéphane Deny. Barlow twins: Self-supervised learning via redundancy reduction, 2021. 2, 5, 6, 8

[83] Jiachen Zhu, Rafael M. Moraes, Serkan Karakulak, Vlad Sobol, Alfredo Canziani, and Yann LeCun. Tico: Transformation invariance and covariance contrast for self-supervised visual representation learning, 2022. 14

A. Appendix Section

A.1. Conditions for Good Representation

The methods for Self-Supervised Learning highlighted above have shown great potential in generating useful visual representation h using data augmentation on input x and then using contrastive loss for comparison. Most of these methods have been benchmarked using standard academic datasets like ImageNet [50] (1.3M images with 1k classes) and Places365 [54] (1.8M images with 365 classes). The practical applicability of contrastive self-supervised learning are mentioned in [25] where the authors have observed four conditions for which self-supervised contrastive learning methods produce good feature representations h . Below we have elaborated the four conditions and how they relate to the downstream application of Handwriting Verification:

1. **Data Quantity:** Limited pre-training data with smaller networks allows for faster and cheaper pre-training since the impact on downstream application is within tolerance. In context of handwriting verification, despite the abundance of unlabeled handwritten images the model should be able to learn good representation h even from a smaller subset of handwritten dataset x .
2. **Pre-Training Domain:** Representations learned during pre-training benefits from having same domain type as the downstream application. Adding representations from other domain generalizes the features space h . In the case of handwriting verification task, we can use CEDAR Letter Handwriting Dataset for feature extraction (pre-training) $f(x)$ since the features generated are within-domain and relevant to the handwritten text. Generalizing feature space h with other non-handwritten text like images from ImageNet [50] which broaden the feature space leading to high variability from unrelated input domains.
3. **Data Augmentation Quality:** With Data Augmentation the input is altered x' to create contrastive examples which helps in learning self-supervised representations. While certain augmentation techniques help enhance generalization within specific domains, it is important to maintain consistency and natural variability for the inherent patterns observed in the handwritten styles. Certain transformations like changing aspect ratio, elastic distortions could alter the handwritten style. Hence, we have empirically evaluated

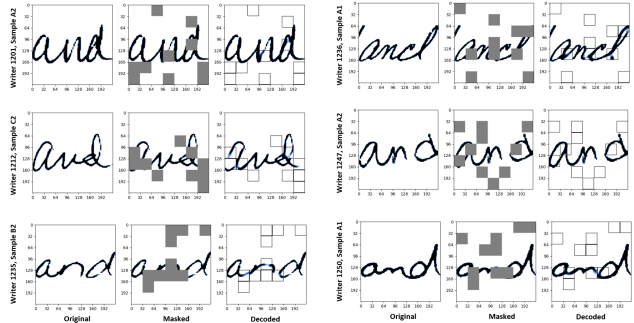


Figure 6. Original, Masked and Decoded handwritten image samples from multiple writers 1471 first sample B with 64x64 size with 32x32 masked patches and masking ratio set to 0.2

the data augmentation techniques for handwriting verification in context of contrastive self-supervised pre-training.

4. **Downstream Task Granularity:** Self-Supervised Contrastive methods have shown better applicability with coarse-grained downstream tasks involving higher-level attributes as compared to fine-grained tasks. Handwriting verification, benefits from both coarse-grained and fine-grained features. Coarse-grained features are responsible in extracting high-level handwriting characteristics such as overall shape, slantness, curvation and spatial layout. Whereas, fine-grained features capture details such as characters shapes (e.g. staff of a), stroke thickness, order, character variations and so on. Hence, in this chapter we show a contrastive self-supervised approach for handwriting verification. This method is pre-trained on unlabeled handwritten dataset $f(x)$ to generate both coarse grained and fine-grained features which represents the individuality of writers $p(y|x_1, x_2)$ within the handwritten domain.

A.2. Related Generative AR Models

PixelRNN [71] uses Long Short Term Memory (LSTM [37]) trained with masked convolutions and multinomial loss function to predict raw pixel values (0-255) as categories. PixelCNN [71] was proposed to make the PixelRNN efficient and capture a fixed size receptive field using convolutional layers.

Gated PixelCNN [72] efficiently uses masked convolutions to model conditional pixel distribution. The masked convolutions replaces the ReLU activation using gated activation function as shown in Equation 17. This allows complex interactions between pixel x_i to be modeled similar to PixelRNN [71].

$$\mathbf{y} = \tanh(\mathbf{W}_f \mathbf{x}) \odot \sigma(\mathbf{W}_g \mathbf{x}) \quad (17)$$

where, σ is sigmoid activation for k^{th} layer and \odot is element wise multiplication between the result of the convolutions between the two receptive fields. PixelCNN++ [63] and PixelSNAIL [22] improves Gated PixelCNN [72], with improvements like using output mean and standard deviations for the logistics instead of softmax in the mixture. PixelCNN have slow sampling rate since product of conditional is a time expensive operation because n^2 forward model propagation is needed. AR models do not explicitly learn the latent representations h like Flow based models or AutoEncoders (AE) but we can still apply feature aggregation techniques to derive hidden representations h .

iGPT [17] more recently has explored the use of autoregressive objectives L_{AR} (e.g. PixelCNN objective [71]) and BERT [28] L_{BERT} objective using transformer architecture. L_{AR} and L_{BERT} have worked well with Large Language Models for natural language (e.g. GPT2 [2] and similar) which uses masks word tokens in its pre-training regime which has shown great generalization and improvement for the downstream task with fewer labels. Given input data X the AR objective L_{AR} was to minimize the negative log likelihood $\mathbb{E}_{x \sim X} [-\log p(x)]$ of input distribution $p(x)$ which is a density function modeled using product of pixel conditionals $\prod_{i=1}^n P(x_i | (x_1, \dots, x_{i-1}))$. iGPT also considers the use of BERT [28] objective L_{BERT} where the model is trained to minimize the negative log-likelihood of $p(x)$ to learn predicting masked part of the input x_m using the unmasked part of the input $x_{[1,n] \setminus M}$ as shown in the Equation shown in Equation 18 below:

$$L_{BERT} = \mathbb{E}_{x \sim XM} \mathbb{E}_{i \in M} [-\log p(x_i | x_{[1,n] \setminus M})] \quad (18)$$

A.3. Related Generative Flow based Models

Flow based generative models explicitly learns the true data distribution $p(x)$ by a sequence of invertible transformation functions $f(x)$ to map input x to latent representation z . Since the transformation are invertible $x = f^{-1}(z)$ is true. [52] provides an intuitive understanding of how flows model input density function $p(x)$ using the Equations 19 below:

$$\begin{aligned} \int p_x(x) dx &= \int p_z(z) dz = 1 && \dots \text{Probability Definition} \\ p_x(x) &= p_h(z) \left| \frac{dz}{dx} \right| = p_z(f(x)) \left| \frac{df(x)}{dx} \right| && \dots \text{Derivative} \\ \log p_x(\mathbf{x}) &= \log p_z(f(\mathbf{x})) + \log \left| \det \frac{df(\mathbf{x})}{d\mathbf{x}} \right| && \dots \text{Logarithm} \end{aligned} \quad (19)$$

It is difficult to find f^{-1} and $\log \left| \det \frac{df(\mathbf{x})}{d\mathbf{x}} \right|$ of complex f hence flow models use sequence of invertible functions $f_{1, \dots, K}$.

NICE [29] Non-Linear Independent Component estimates $p(x)$ uses an easy invertible function f^{-1} and easy jacobian $\log \left| \det \frac{df(\mathbf{x})}{d\mathbf{x}} \right|$ computation. NICE uses dequantized version of input images x by adding uniform noise u and re-scaling input data between $[-1, 1]$ to prevent degenerate solution because of infinite high likelihood placed on discrete points. NICE separates dequantized input space into odd $x_1^{(i)}$ and even $x_2^{(i)}$ dimensions. Coupling function is then applied as shown in Equation 20 below:

$$\begin{aligned} z_1^{(i)} &= x_1^{(i)} \\ z_2^{(i)} &= x_2^{(i)} + m^{(i)} x_1^{(i)} \\ z &= \exp(s) \odot z^{(4)} \end{aligned} \quad (20)$$

Each coupling layers $m^{(i)}$ ($i=1$ to 4) have rectified linear units. The output of m^4 coupling layer is element-wise multiplied by scaling matrix s to preserve the relative importance across dimensions in x . The loss is the negative log likelihood of Equation 2.

RealNVP [30] uses real-valued non-volume preserving transformations f which are stable, invertible and learnable for computing exact $p(x)$. Similar to NICE [29], RealNVP aims to provide a tractable and flexible solution to computing Jacobian determinant of the transformation. RealNVP uses affine coupling layer on input x with dimensionality D as shown in Equation 21 below:

$$\begin{aligned} y_{1:d} &= x_{1:d} \\ y_{d+1:D} &= x_{d+1:D} \odot \exp(s(x_{1:d})) + t(x_{1:d}) \end{aligned} \quad (21)$$

where, s and t stands for scale and translation. The Jacobian of the affine coupling is the product of diagonals which are efficiently computed to be independent of scale s and translation t . RealNVP uses deep convolutional neural networks to make complex s and t . It uses masked convolutions to exploit the local correlation within input image and couples layers in an alternating pattern to overcome stagnant output post transformation. It also uses multi-scale architecture to overcome the problem of high-compute needed to generate high dimensional latent space z . It applies squeezing and split operation to reduce the dimensionality of the image by certain factor as needed. Similar to NICE [29], the loss function is simply the negative log likelihood of Equation 2. Similar, to Nice and RealNVP, Glow [47] proposes to use invertible 1x1 convolution within coupling function. Within handwritten verification domain, a flow based model helps in capturing characteristics of the handwriting, such as stroke patterns, curvature and other writing styles which can be used as latent features by a discriminator network for generating a similarity metric.

A.4. Related VAE based Models

Within VAE, latent representations z are sampled from an approximate posterior $q_\phi(z|x) = \mathcal{N}(\mu, \sigma^2)$. The en-

coder represents input x using z with help of a normal distribution with mean function μ and standard deviation as σ^2 . Posterior collapse happens when μ and σ collapse to a constant values C_μ and C_σ . Hence, approximate posterior distribution $q_\phi(z|x)$ is only dependent on prior $q_\phi(z)$ which is fixed to a normal distribution of $\mathcal{N}(C_\mu, C_\sigma^2)$. The result of the collapse, is that the latent representation z becomes independent of x thereby the decoder only samples noisy z samples from a incorrect approximate posterior $q_\phi(z) = \mathcal{N}(C_\mu, C_\sigma^2)$. This makes the decoder impossible to use the information x from the latent representation z . Many approaches have been proposed in the literature to tackle the problem of posterior collapse using KL annealing for task-specific representation learning: Generating sentences [12], sketch-rnn [40], dilated convolutions in VAW [79], AG-CVAE [76]. More recently, Ladder VAE [68], fixing ELBO [1], VQ-VAE [74] have been proposed to help tackle the collapse problem with VAE.

VQ-VAE [74] is one of the notable mentioned within the VAE family of models. VQ-VAE is a discrete latent VAE model. VQ-VAE merges auto-regressive distributions within the decoder. VQ-VAE defines a codebook of latent embedding space e with size K and dimensionality D . Input x is passed into encoder to generate latent representation $z_e = t_{enc}(x)$. The representation z_e is discretized z_q using the codebook e by mapping z_e to the nearest element in embedding e_j using l_2 distance $z_q = \operatorname{argmin}_j \|z_e - e_j\|_2$. During forward propagation nearest $z_q(x)$ is passed to the decoder $f_{dec}(z_q)$. While in backward pass the gradient the gradients are unaltered and passed to encoder. VQ-VAE loss is as shown in the Equation 22 below:

$$L = \log p(x | z_q(x)) + \|sg[z_e(x)] - e\|_2^2 + \beta \|z_e(x) - sg[e]\|_2^2 \quad (22)$$

First term in Equation 22 is the reconstruction loss used by the encoder and decoder to reconstruct input x from $z_q(x)$. The second term is the l_2 error to update the embedding vector e_i closer to $z_e(x)$ which is used to optimize the embeddings and the last term is a commitment loss to make sure that the encoder output $z_e(x)$ grows in same proportion as the codebook embeddings e . sg stop gradient is identity at forward compute and zero derivatives during gradient computation. VQ-VAE2 [62] was proposed as an improvement to generate synthetic samples of higher coherence and fidelity using multi-scale hierarchical organization of VQ-VAE with priors over latent variables which generated samples that rival Generative Adversarial Networks [36] (GANs) on ImageNet [50] datasets.

A.5. Related SimCLR and Contrastive based Models

Although, SimCLR got state-of-the-art SSL performance on standard datasets like ImageNet there are some

weaknesses like sensitivity to augmentation techniques and need for large batch size with lot of negative examples to improve performance. Building on top of SimCLR are many approaches are: **Decoupled Contrastive Learning** (DCL) [80] which defines a DCL loss by removing the positive pairs from the denominator of the InfoNCE [73] loss. **Nearest Neighbor Contrastive Learning** (NNCLR) [33] also builds upon the idea from SimCLR [18] and have proposed to use nearest-neighbours to get diverse set of positive pairs. Other interesting approaches to contrastive SSL are: Swapping Assignment with multiple Views (SWAV) [13], Masked Siamese Networks (MSN) [5], Prior Matching for Siamese Networks (PMSN) [4], Synchronous Momentum Grouping (SMoG) [57], Transformation Invariance and Covariance Contrast (TiCo) [83], Self-Supervised Learning of Maximum Manifold Capacity Representations (MMCR) [81].